**This is a preprint version of the paper published: In ASME International Mechanical Engineering Congress and Exposition, vol. 86717, p. V009T13A006. American Society of Mechanical Engineers, 2022.
https://doi.org/10.1115/IMECE2022-95590

DRFAT: BARBED MICRONEEDLE DESIGN TO ENHANCE PENETRATION AND RETRACTION FORCES USING FINITE ELEMENT MODELLING

Ranjith D. Janardhana [1], Mateus Cabanlong[1], Pavan Muttil [2] and Nathan Jackson [1]

[1]Department of Mechanical Engineering, University of New Mexico, Albuquerque, NM, USA
[2] College of Pharmacy, University of New Mexico, Albuquerque, NM, USA

ABSTRACT

Nature has optimized the structure of needles to reduce penetration force and increase retraction force as demonstrated by honeybee stingers, mosquitos and porcupines. Current microneedles typically consist of smooth sharp tips to reduce penetration forces, but these have poor retraction forces. This paper investigates the design of a bio-inspired barbed microneedle and its effects on insertion and retraction forces on the outer and inner layers of the skin. Various microneedle designs were investigated using COMSOL Multiphysics software to determine the impact of needle tip sharpness and barbed design on the forces. The interlocking of the microneedle with skin tissue was higher in the case of barbed-shaped microneedle compared to barbless needle resulting in a higher retraction force. Also, the size and geometry of the microneedle design affect the insertion and retraction forces characteristics. The development of a finite element model will allow us to further enhance the design of bio-inspired microneedles. This work also demonstrates the feasibility of using microfabrication techniques to manufacture various barbed microneedle designs using Su-8 based microneedles.

Keywords: Barbed microneedle, penetration force, finite element modeling, retraction force, painless microneedle, Su-8 microneedle

NOMENCLATURE

F	force (N)
σ	stress (N/m^2)
A	cross-section area of the needle (m^2), πr^2
r	radius of the needle (μm)
x	longitudinal direction (μm)
y	transverse direction (μm)

1. INTRODUCTION

The conventional hypodermic needles used for transdermal drug delivery typically result in a painful insertion, which is not desired by numerous patients [1]. Microneedles (MNs) were initially developed as a "painless" alternative and has been extensively researched over the past few decades to deliver various drugs and vaccines with minimal pain [2–5]. They have numerous designs which are usually limited by their manufacturing methods and can be made from various materials, including metals, ceramics, polymers, and glass. Manufacturing methods include microfabrication, 3D printing, glass pulling, mold casting and various other techniques. Further, MNs can consist of solid, hollow, or dissolvable materials depending on the mechanism of drug delivery [6].

Currently, most MNs are manufactured to have smooth edges to reduce penetration and retraction forces to reduce the pain involved. However, recently there has been a need to develop a slow controlled drug release mechanism, so the drugs are delivered over an extended period. Most MNs consist of sharp smooth surfaces which are good to reduce penetration forces, but they have a poor retraction force due to low tissue adhesion [7]. Lower retraction force allows the needle to be easily removed from the skin, preventing the MN from being applied for a long period. Therefore, there is a need to design a new MN shape that can improve tissue adhesion. Studies have demonstrated that biomimetic design inspired by bee stingers and mosquitos, consisting of a barbed-shaped MN resulted in an increased retraction force [8–11]. In this regard, the current work was focused on MN design and exploring the effects of flat barbed MN on the insertion and retraction force. However, the development of bioinspired MNs needs to consider not only the design but method of manufacturing. The manufacturing method should be batch fabrication compatible, be low cost, and be able to make MNs out of various materials.

Successful delivery of drugs through the skin, requires the MNs to penetrate through the stratum corneum (outer layer of the skin) and puncture the dermis layer with minimum bending or buckling of the needle [12]. Various aspects affect the force required to penetrate the skin, such as the velocity of insertion, shape of the needle, material properties of the needle, and mechanical properties of the skin which vary based on location, gender, age, and dryness [13–15]. Solid MNs involved in this study can transfer drugs through the poke and patch method [16], dissolving coated drug [17], or dissolving the drug embedded in the needle [18]. Therefore, the control rate of insertion of the MN through the skin to the desired depth is an important factor to be considered during MN design for the targeted drug delivery.

In the paper, we developed a Finite Element Model (FEM) using COMSOL Multiphysics to investigate the insertion and retraction forces of various MN designs. The designs include using traditional MN that have simulation and experimental data [11] to validate models. We investigated the effects of varying the sharpness and shape of the needle as well as designing a basic barbed needle MN. The materials, properties, parameters, and other conditions were held constant but could be investigated in the future. The goal of this paper was to develop the FEM model, validate it, and demonstrate a proof-of-concept barbed MN that can be used to increase retraction force after skin penetration. The paper also demonstrates the capability of fabricating both types of devices using various manufacturing techniques. Planar microfabrication methods has a potential of creating high resolution (1μm) feature sizes with a high aspect ratio; further, MNs can be created using various materials through the molding process such as dissolvable needles.

2. MATERIALS AND METHODS

2.1 Computational Domain

In this work, four MN designs were studied and named: design 1, design 2, design 3, and design 4. Figure 1 shows the basic concept for the 2D FEM consisting of the two skin layers and the MN. Figure 1 also shows the dimensions and shape of the MN used in design 1, whereas designs 2-4 were shown in Fig. 2. Design 1 was based on a previously reported design that had experimental and simulation data [11], design 2, 3 and 4 were ultrasharp MNs with a 1 μm tip. Design 1 consisted of a trapezoidal shape MN with a 20 μm tip and a taper angle of 5.14°. Design 4 was similar to design 3 but had a narrower taper tip. Design 3 and 4 both had a single triangular shaped barb on each side of the needle with a 45° taper. Design 2, 3, and 4 have a trapezoidal tip that is 200 μm in length and 1μm tip, and then a rectangular shaft of length 400 μm. Design 1 was used to validate the model by comparing it to previous literature results.

The base diameter and needle tip diameter for design 1 were 200 μm and 20 μm, respectively, as shown in Fig. 1a and 1b. The length was 1000 μm and the tapered angle at the needle tip was 5.14° (Fig. 1b). Figure 2a shows the dimensions of the MN design 2 with base width, tip diameter and total length of 100 μm, 1 μm and 600 μm, respectively. The length of the tapered shape of design 2 was 200 μm and the angle at the tip was 13.9°. Design 3 was identical to design 2 except for the flat triangular barbed attached to the base diameter at a distance of 40 μm from the needle tip as illustrated in Fig. 2b. The barb design is shown in Fig. 2b. Design 4 combined design 1 (narrow taper) with design 3 barb. The dimensions of design 4 are shown in Fig. 2c.

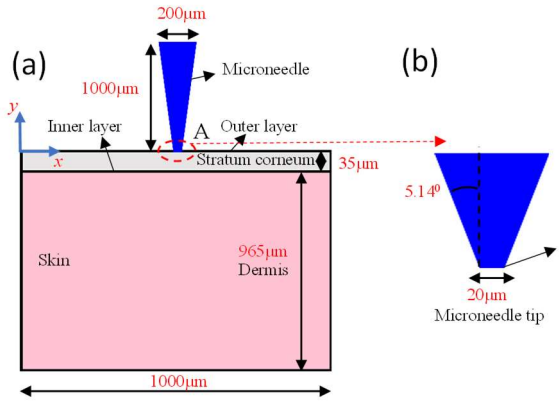

FIGURE 1. a) COMPUTATIONAL DOMAIN FOR MN DESIGN 1 WITH SKIN AND b) ZOOMED VIEW OF MN TIP SECTION.

The FEM domain for the skin was split into two layers: stratum corneum and dermis layer, as shown in Fig. 1a. The stratum corneum is the outer layer of the skin which had a thickness of 35 μm followed by the dermis layer that had a thickness of 965 μm, to make the entire skin thickness 1 mm. Hereafter, the upper layer of the stratum corneum will be referred as the "outer layer" and the upper layer of the dermis will be referred to as the "inner layer" for simplicity (Fig. 1a). The total dimension of the skin was 1000 μm×1000 μm.

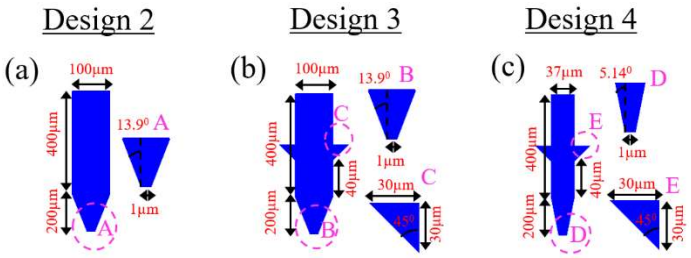

FIGURE 2. DIMENSIONS OF a) MN DESIGN 2 WITH ZOOMED VIEW OF MN TIP SECTION, b) MN DESIGN 3 WITH ZOOMED VIEW OF MN TIP SECTION AND BARBED DESIGN RESPECTIVELY AND c) MN DESIGN 4 WITH ZOOMED VIEW OF MN TIP SECTION AND BARBED DESIGN RESPECTIVELY.

2.2 Mesh and Boundary Conditions

Figures 3a and 3b show the example of the computational mesh along with the boundary condition used for design 1. Symmetry was used so that only half of the computational geometry was simulated to increase computational efficiency. The triangular mesh was used for MN whereas quadrilateral mesh was applied to the skin layers. The mesh for the skin consists of two structure blocks (Block 1 and Block 2), as indicated in Fig. 3. Block 1 had finer mesh than block 2. The bottom and left sides of the domain were enforced with fixed boundary conditions. Mesh details were provided in the Table 1.

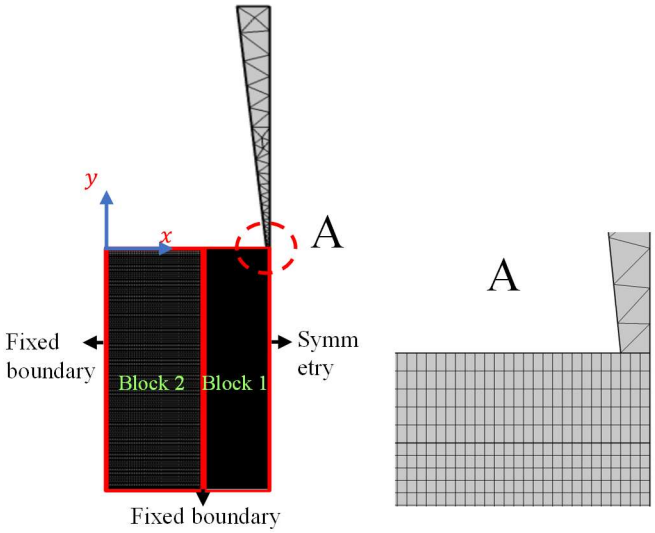

FIGURE 3. MESH FOR THE a) MN DESIGN 1 ALONG WITH BOUNDARY CONDITION ZOOMED VIEW OF AREA "A" NEAR NEEDLE TIP.

TABLE 1. MESH DEATAILS FOR HALF OF THE DOMAIN.

	Needle	Skin
	Number of elements	
Design 1	59	20500
Design 2	108	23920
Design 3	140	23920
Design 4	113	23920

2.3 Numerical Simulation

Numerical analysis was conducted by FEM using COMSOL Multiphysics software to understand the skin behavior under different MN designs. Time-dependent simulations were performed in two stages: "insertion" and "retraction". Insertion refers to the penetration of the MN into the skin layers, whereas retraction refers to the extraction of the MN from the skin. The MN was inserted to a depth of 500 µm with a needle velocity of 0.5mm/s. Initially, the MN was touching the surface of the skin at a depth of zero (y = 0) and $t = 0$. Similarly, the MN was retracted from the skin at a depth of 500 µm, assuming that no hole was created from the penetration, with a needle velocity of 0.5 mm/s. The retraction process was continued until the needle was completely removed from the skin. The insertion force required to puncture the skin was calculated from maximum stress acting on the outer and inner layers of the skin. The force was then determined from the stress and area that was in contact with the skin. The retraction force was also calculated similar to the insertion force for both outer and inner layers of the skin.

Silicon was used as the MN material because it is extensively used experimentally. The properties of the skin were previously reported [11]. Table 2 provides details about the material properties of MN and skin. A viscoelastic model was used to represent both layers of the skin. The contact pair established between MN surface and skin layers used a penalty method algorithm [11].

TABLE 2. MATERIAL PROPERTIES OF MN AND SKIN LAYERS

Properties	Silicon MN	Stratum corneum	Dermis
Young's Modulus (kPa)	170 x 10^6	3400	34
Poisson's ratio	0.28	0.48	0.48
Density (kg/m^3)	2329	1300	1200

2.4 Microfabrication of Barbed Microneedles

Microfabrication techniques were used to demonstrate the capability of fabricating planar barbed MNs. Two types of MNs were fabricated 1) Su-8 MNs and 2) dissolvable (polyacrylic acid (PAA)) polymer-based MNs. Both devices were fabricated using a (100) silicon substrate that was cleaned using standard Radio Corporation of America (RCA) cleaning methods. The Su-8-based MNs were fabricated by first depositing a thin layer of omnicoat which acted as a release layer for the Su-8. Then a 100 µm thick layer of Su-8 3050 was spin coated at 1500 rpm onto the wafer. The Su-8 layer was patterned to create the barbed MN and released from the substrate. Using photolithography any design of MN or barbed dimensions is feasible and could be designed in the future.

Dissolvable MNs were fabricated using soft lithography by creating a Su-8 on a silicon master mold. Similar to the methods described above, a thick Su-8 layer was deposited and patterned to have the opposite polarity as the above Su-8 MNs. The thickness of the MNs can be easily modified by adjusting the spin speed or altering the viscosity of the Su-8. Once the master mold was created, the PAA was dispensed in the mold and allowed to cure in the desiccator. The PAA MNs were then removed from the mold. This process allows the master mold to be used multiple times, thus making the process batch fabrication compatible. In addition, the soft lithography method can be used to make various other polymeric MNs.

3. RESULTS AND DISCUSSION

The numerical analysis of design 1 was compared with previous results to validate the model [11]. Figure 4 represent the insertion and retraction forces acting on the outer and inner layer of the skin for design 1. At point "P_1", the insertion force drops sharply and increases gradually thereafter. This point was treated as the initial penetration force required to tear the outer layer of the skin according to other experimental and numerical studies [9,11,20] for different MN design. The numerical results obtained for design 1 were in agreement with those obtained with Chen et al. [11] as depicted in Fig. 4. After penetration the force continues to increase due to the mass of the needle and increased width of the MN base as it was inserted into the skin. The MN displacement at penetration was larger than the thickness of the outer layer due to buckling or bending of the skin. The retraction force initially increases (in the opposite direction) as shown in Fig. 4, and then decreases as the needle was extracted from the skin due to the reduction in the area of the needle. The retraction force was noted as "R_1" in the figure, as indicated in Fig. 4. Similar tendencies were observed for insertion and retraction

force profiles in the experimental results from previous studies [7,9,11] under different conditions and for various MN designs. The initial penetration and retraction forces for design 1 were 48 mN and 26mN respectively. Figure 5 demonstrates the insertion and retraction forces on the inner layer of the skin. The inner layer of skin required a much lower insertion force of 4.2 mN, need to penetrate the outer layer first. The retraction force was also significantly lower for the inner layer, because the MN needs to retract from the outer layer to be fully retracted from the skin. The results from Fig. 4 and 5 represent that the stratum corneum (outer layer) was the major barrier to both piercing the skin and retracting the MN from the skin.

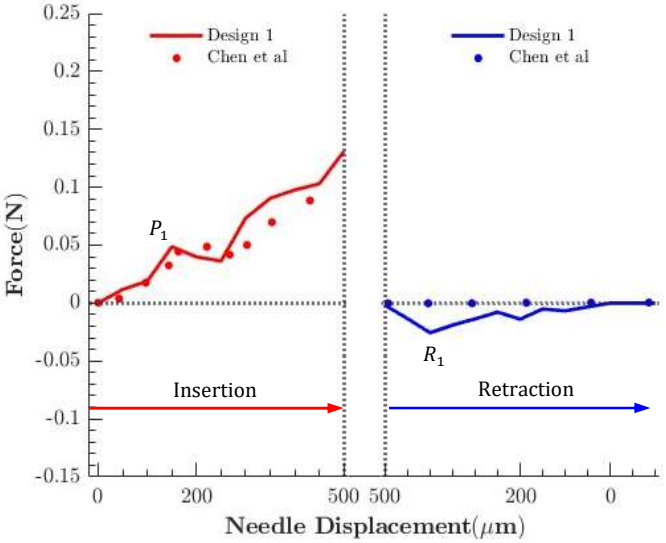

FIGURE 4. INSERTION AND RETRACTION FORCES ON THE OUTER LAYER OF THE SKIN FOR THE MN DESIGN 1.

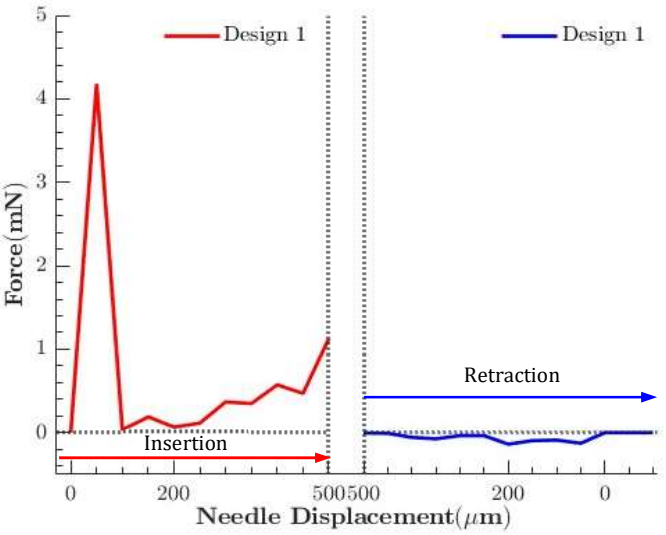

FIGURE 5. INSERTION AND RETRACTION FORCES ON THE INNER LAYER OF THE SKIN FOR THE MN DESIGN 1.

The simulation results of MN design 2, 3 and 4 are shown in Fig. 6 and 7 under similar conditions used for design 1. The MN design ~~2~~ 3 exerts a maximum insertion force and retraction

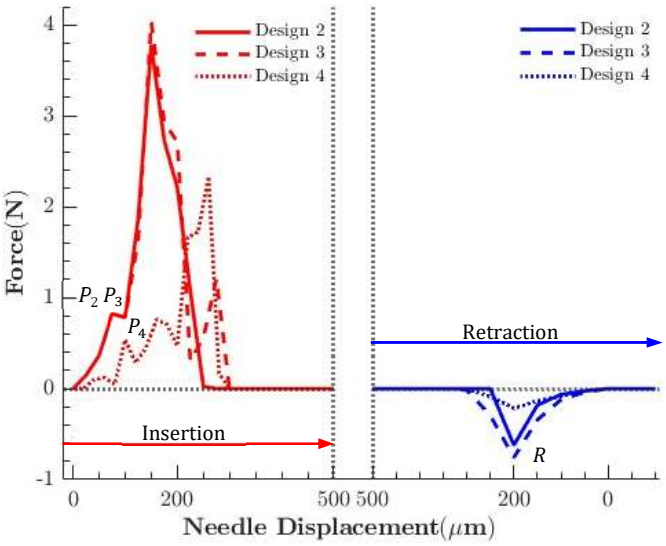

FIGURE 6. INSERTION AND RETRACTION FORCES ON THE OUTER LAYER OF THE SKIN FOR THE MN DESIGN 2, 3 AND 4.

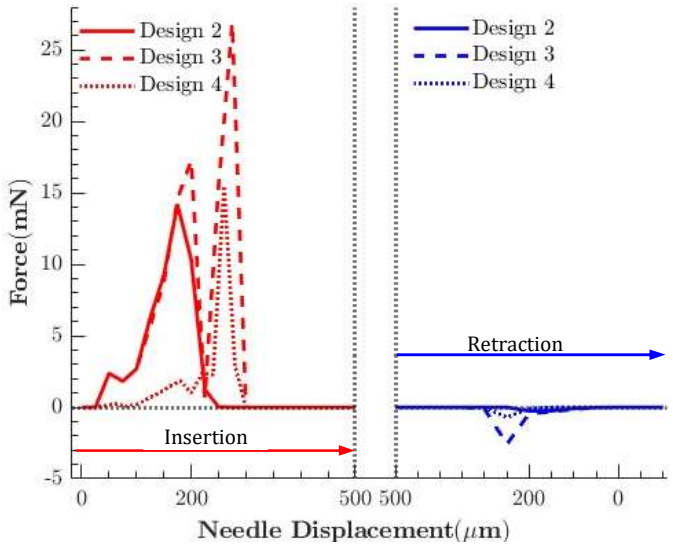

FIGURE 7. INSERTION AND RETRACTION FORCES ON THE INNER LAYER OF THE SKIN FOR THE MN DESIGN 2, 3 AND 4.

force compared to the other designs, whereas design 4 experiences the least force due to the sharper taper of the MN. The insertion force initially increases in all three designs and the points "P_2", "P_3" and "P_4" demonstrate penetration forces for the different designs. The peak forces for design 3 and 4 were altered due to the barbed design in comparison with design 2. The taper angle appears to significantly impact the insertion force where a sharper (narrower) taper resulted in a reduced penetration force as expected. The identical behavior was observed for the retraction forces with peak forces -0.62N, -0.76N and -0.22N (at point R) for designs 2, 3 and 4, respectively, as presented in Fig. 6. These peak forces correspond to the maximum retraction force required to extract the needle from the skin. Fig. 7 shows the insertion and retraction forces acting on the inner layer of the skin for designs 2, 3 and 4. The inner layer of the skin

experiences minimum insertion and retraction forces similar to the design 1. In all cases, the barbed MNs demonstrated increased retraction force compared to the barbless MN.

The base geometry of the MN design 3 was identical to design 2 with additional barbed as illustrated in Fig. 2a and 2b. The insertion and retraction forces increased due to the adhesion of the tissue with the barbed structure compared to the smooth surface of design 2. The tapered angle of design 2 and design 3 were 13.9° and design 4 was 5.14° (Fig 2). The penetration force and retraction force on both the outer and inner layers decreased for design 4 due to the change in tapered angle at the needle tip in comparison with the other designs. Design 1 consists of a complete tapered shape with an increase in cross-sectional area, whereas other designs consist of a tapered shape up to 200 µm and thereafter a straight profile. From the insertion force and retraction force results, it was demonstrated that the shape of the MN also effects the retraction and penetration forces on the skin. Previous experimental studies have demonstrated that barbed MN can reduce penetration force and increase retraction force. Further studies of optimal barb dimensions and locations are needed to optimize needle performance.

To summarize, the simulation results of the design 1 MN was similar to the previous result [11], thus validating the model. Creating a sharper tip with a lower taper angle resulted in a decrease in penetration and retraction forces. The barbed MNs resulted in increased retraction force.

The ability to fabricate barbed microneedles with various barbed designs and needle shapes was demonstrated in Fig. 8. The Figure 8 demonstrates the feasibility of fabricating various shaped MNs and barb designs, which can be created by altering the lithography mask design, changing the geometry of the MN by varying the dimensions of the barb.

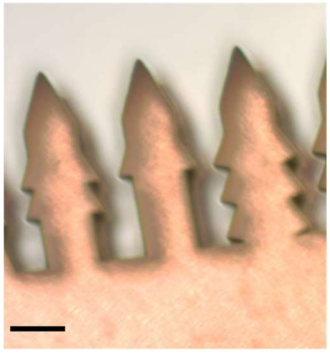

FIGURE 8. FABRICATED SU-8 BARBED MICRONEEDLES WITH VARIOUS BARBED DESIGNS. SCALE BAR IS 50 mm.

In the future, the above microfabrication procedure can be used to achieve the ultra-shape MNs (design 2, 3 and 4) and tested experimentally to validate the above FEM model. These validations further allow to enhance the design of the microneedles using various materials such as polymers, ceramics, glass or metal.

4. CONCLUSION

The insertion force on the stratum corneum (outer layer) was within 4 N with all four MN designs. The retraction force increased due to improved skin tissue adhesion with barbed design. The tip angle also affected the insertion and retraction forces. Previous studies [3] demonstrated that pain response was associated with insertion force; therefore, reducing insertion force is critical. In addition, having a high retraction force can prevent the MN from being easily removed, which is ideal when long-term application is required. This paper demonstrates that barbed MN can be used to increase retraction force, and we believe that they can also be designed to reduce penetration force, similar to the naturally occurring bee stinger which requires further experimental studies. The current study also demonstrated that the high-resolution barbed MN can be fabricated using standard microfabrication techniques. Future work may involve validating the FEM simulation with experimental results and optimizing the size and geometry of the barb-shaped design with reduced penetration and increased retraction forces.

ACKNOWLEDGEMENTS

The authors would like to thank all members of the SMART Laboratory group at University of New Mexico.

REFERENCES

[1] Davis, S. P., Landis, B. J., Adams, Z. H., Allen, M. G., and Prausnitz, M. R., 2004, "Insertion of Microneedles into Skin: Measurement and Prediction of Insertion Force and Needle Fracture Force," J. Biomech., **37**(8), pp. 1155–1163.

[2] Kim, Y.-C., Park, J.-H., and Prausnitz, M. R., 2012, "Microneedles for Drug and Vaccine Delivery," Adv. Drug Deliv. Rev., **64**(14), pp. 1547–1568.

[3] Gill, H. S., Denson, D. D., Burris, B. A., and Prausnitz, M. R., 2008, "Effect of Microneedle Design on Pain in Human Subjects," Clin. J. Pain, **24**(7), p. 585.

[4] Haq, M. I., Smith, E., John, D. N., Kalavala, M., Edwards, C., Anstey, A., Morrissey, A., and Birchall, J. C., 2009, "Clinical Administration of Microneedles: Skin Puncture, Pain and Sensation," Biomed. Microdevices, **11**(1), pp. 35–47.

[5] Kaushik, S., Hord, A. H., Denson, D. D., McAllister, D. V., Smitra, S., Allen, M. G., and Prausnitz, M. R., 2001, "Lack of Pain Associated with Microfabricated Microneedles," Anesth. Analg., pp. 502–504.

[6] Dharadhar, S., Majumdar, A., Dhoble, S., and Patravale, V., 2019, "Microneedles for Transdermal Drug Delivery: A Systematic Review," Drug Dev. Ind. Pharm., **45**(2), pp. 188–201.

[7] Han, D., Morde, R. S., Mariani, S., La Mattina, A. A., Vignali, E., Yang, C., Barillaro, G., and Lee, H., 2020, "4D Printing of a Bioinspired Microneedle Array with Backward-Facing Barbs for Enhanced Tissue Adhesion," Adv. Funct. Mater., **30**(11).

[8] Ling, J., Jiang, L., Chen, K., Pan, C., Li, Y., Yuan, W., and Liang, L., 2016, "Insertion and Pull Behavior of Worker Honeybee Stinger," J. Bionic Eng., **13**(2), pp.

303–311.
[9] Ling, J., Song, Z., Wang, J., Chen, K., Li, J., Xu, S., Ren, L., Chen, Z., Jin, D., and Jiang, L., 2017, "Effect of Honeybee Stinger and Its Microstructured Barbs on Insertion and Pull Force," J. Mech. Behav. Biomed. Mater., **68**(August 2016), pp. 173–179.
[10] Cho, W. K., Ankrum, J. A., Guo, D., Chester, S. A., Yang, S. Y., Kashyap, A., Campbell, G. A., Wood, R. J., Rijal, R. K., Karnik, R., Langer, R., and Karp, J. M., 2012, "Microstructured Barbs on the North American Porcupine Quill Enable Easy Tissue Penetration and Difficult Removal," Proc. Natl. Acad. Sci. U. S. A., **109**(52), pp. 21289–21294.
[11] Chen, Z., Lin, Y., Lee, W., Ren, L., Liu, B., Liang, L., Wang, Z., and Jiang, L., 2018, "Additive Manufacturing of Honeybee-Inspired Microneedle for Easy Skin Insertion and Difficult Removal," ACS Appl. Mater. Interfaces, **10**(35), pp. 29338–29346.
[12] Makvandi, P., Kirkby, M., Hutton, A. R. J., Shabani, M., Yiu, C. K. Y., Baghbantaraghdari, Z., Jamaledin, R., Carlotti, M., Mazzolai, B., Mattoli, V., and Donnelly, R. F., 2021, *Engineering Microneedle Patches for Improved Penetration: Analysis, Skin Models and Factors Affecting Needle Insertion*, Springer Singapore.
[13] Benítez, J. M., and Montáns, F. J., 2017, "The Mechanical Behavior of Skin: Structures and Models for the Finite Element Analysis," Comput. Struct., **190**, pp. 75–107.
[14] Kalra, A., and Lowe, A., 2016, "An Overview of Factors Affecting the Skins Youngs Modulus," J. Aging Sci., **4**(2).
[15] Davis, S. P., Prausnitz, M. R., and Allen, M. G., "Fabrication and Characterization of Laser Micromachined Hollow Microneedles," *TRANSDUCERS '03. 12th International Conference on Solid-State Sensors, Actuators and Microsystems. Digest of Technical Papers (Cat. No.03TH8664)*, IEEE, pp. 1435–1438.
[16] Mikszta, J. A., Alarcon, J. B., Brittingham, J. M., Sutter, D. E., Pettis, R. J., and Harvey, N. G., 2002, "Improved Genetic Immunization via Micromechanical Disruption of Skin-Barrier Function and Targeted Epidermal Delivery," Nat. Med., **8**(4), pp. 415–419.
[17] Lee, J. W., Park, J.-H., and Prausnitz, M. R., 2008, "Dissolving Microneedles for Transdermal Drug Delivery," Biomaterials, **29**(13), pp. 2113–2124.
[18] Shirkhanzadeh, M., 2005, "Microneedles Coated with Porous Calcium Phosphate Ceramics: Effective Vehicles for Transdermal Delivery of Solid Trehalose," J. Mater. Sci. Mater. Med., **16**(1), pp. 37–45.
[19] COMSOL Multiphysics® v. 6., "COMSOL AB, Stockholm, Sweden.," COMSOL AB, Stock. Sweden. [Online]. Available: www.comsol.com.
[20] Kong, X. Q., Zhou, P., and Wu, C. W., 2011, "Numerical Simulation of Microneedles' Insertion into Skin," Comput. Methods Biomech. Biomed. Engin., **14**(9), pp. 827–835.